Journal of Petroleum Science and Engineering 196 (2021) 107661

Contents lists available at ScienceDirect

Journal of Petroleum Science and Engineering

journal homepage: http://www.elsevier.com/locate/petrol

The probability of oil and water movement in tight sandstone: Evaluation methodology and mechanism analysis

Caoxiong Li [a], Mian Lin [b,c,*], Jing Liu [d], Chenggang Xian [a,**], Lili Ji [b], Wenbin Jiang [b]

[a] Unconventional Oil and Gas Science and Technology Institute, China University of Petroleum, Beijing, 102249, China
[b] Institute of Mechanics, Chinese Academy of Sciences, Beijing, 100190, China
[c] School of Engineering Science, University of Chinese Academy of Sciences, Beijing, 100049, China
[d] Schlumberger, Beijing, 100015, China

ARTICLE INFO

Keywords:
Tight oil
Tight sandstone
Fractals
Mineral components

ABSTRACT

The mechanisms of oil and water movement in tight sandstone are complicated. Many factors, like pore structure, mineral component, liquid behavior and environment condition, have great influence on this oil and water movement process. The key influencing factors are still not fully revealed. In this work, we introduced fractal theory into pore space representation process, and then provided an effective model to evaluate the movement probability of oil and water in tight sandstone. This model has considered dominant influencing factors, like mineral wettability, pore roughness, and the behavior of pore space and liquid. On the basis of this model, the mobilization probability within different pores are discussed under different conditions. And finally, as a simple application, the mobilization probability is derived in different depth with complicated formation environment, which provides a new way to evaluate the oil and water mobilization mechanism in tight formation.

1. Introduction

In tight oil reservoir, hydrocarbon is often accumulated and mobilized within a relatively low permeability matrix. For tight sandstone, the typical permeability is lower than 0.1mD (Masters, 1979; Spencer, 1989) and pore throat sizes ranges from approximately 0.03 μm–2 μm. The oil-water mobilization process in tight sandstone is special (Lu et al., 2018). In tight matrix, the influence of pore connectivity, mineral distributions and oil/water flowing behavior are much more obvious and complicated than normal sandstone (Wang et al., 2019; Zhang et al., 2019). The matrix of tight sandstone is combined by different mineral granules, additionally, the cement and dissolution of granules make the matrix more complicated. Typical pores in tight sandstone are interparticle, intragranular, intercrystalline, and dissolution pores (Xiao et al., 2018). These pores exist within mineral grains or between multiple mineral grains. Different mineral grains have different wettability and roughness. The influence of these minerals (especially clay minerals) on multiphase mobilization is not negligible. Cai et al. (2020) pointed out that the influence of clay mineral components has great influence on water mobilization process in tight sandstone based on a series of experiments. In most studies for tight sandstone, the wettability is regarded as macroscopic average value (Liu et al., 2015; Zhang et al., 2016). For microscopic oil-water mobilization calculation, the wettability difference for different grains should be considered. So does the roughness, microscopic resistance and other flowing related parameters.

Tight sandstone has a relatively complex pore space (Zhao et al., 2015), and the characteristic of pore space is greatly influenced by minerals. In the past few years, several pore space reconstruction-related models and methods have been provided, such as the mesh topology model (Krakowska et al., 2014), percolation model (Yong et al., 2013; Ghanbarian et al., 2016) and pore space skeletonization model (Krakowska, 2019). Most of these model can precisely rebuild the pore space, but with low calculation efficiency. Also, the distribution of granules has often been ignored, which may not be suitable for mineral-granules-constructed tight sandstones. Fortunately, pores in tight sandstone possess fractal properties at a certain scale (Katz and Thompson, 1985), as confirmed by the results of mercury injection (Lai and Wang, 2015; Li et al., 2017a; Zhang et al., 2017), magnetic resonance imaging (Zhang and Weller, 2014; Shao et al., 2017a,b; Zhou and Kang, 2016), and SEM/CT image statistical analysis (Tang et al., 2016), similar to mineral grains (Erzan and Güngör, 1995). The pore space reconstruction process can be greatly simplified by using self-similar

* Corresponding author. Institute of Mechanics, Chinese Academy of Sciences, Beijing, 100190, China.
** Corresponding author. Unconventional Oil and Gas Science and Technology Institute, China University of Petroleum, Beijing, 102249, China.
E-mail addresses: linmian@imech.ac.cn (M. Lin), xianchenggang@cup.edu.cn (C. Xian).

https://doi.org/10.1016/j.petrol.2020.107661
Received 16 March 2020; Received in revised form 12 July 2020; Accepted 14 July 2020
Available online 22 July 2020
0920-4105/

properties, so does fractures (Sheng et al., 2019). Balankin, Elizarraraz (Balankin and Elizarraraz, 2012a) rebuilt a fractal continuum model to represent porous media and provided a series of methods to calculate the transport behavior (Balankin and Elizarraraz, 2012b). Pia, Sanna (Pia and Sanna, 2014a) developed an intermingled fractal unit (IFU) method, and used to investigate the transfer problem in porous media (Pia, 2016; Pia and Sanna, 2014b; Pia et al., 2014, 2016). The IFU method is revised from the fractal Sierpinski carpet. The IFU simulates the pore size distribution of real sandstone. Li developed the 3D intermingled fractal model (3D-IFM) to calculate permeability in shale (Li et al., 2017b, 2018a).

Multiphase flow behavior is another fundamental problem during tight oil play formation and development. More complicated than single-phase flow, multiphase flow will introduce interphase or meniscus movement. Thus, the wettability, capillary force, and roughness should be taken into consideration (Yan et al., 2019). One of the traditional multiphase flow models is imbibition in parallel tube bundle theory. A series of models has been developed based on this theory (Meng et al., 2019; Li et al., 2018b). Bryant, Cade (Bryant and Cade, 1992) introduced stress deformation into the parallel tube bundle model and calculated the relative permeability. Blunt (1997) extended it into a three-dimensional network and provided the relative permeability and capillary pressure calculation method. Mani, Mohanty (Mani and Mohanty, 1998) developed the displacement process into a three-dimensional one. Wang, Sheng (Wang and Sheng, 2018) developed a network for multiphase displacement considering threshold pressure gradient. However, pores are scattered randomly in sandstone, unlike in the capillary bundle model. Li, Lin, Ji, Jiang (Li et al., 2019) introduced the mineral component into the 3D-IFM model for tight sandstone and calculated the influencing factors on multiphase displacement.

The purpose of this work is to derive a method to fast evaluate the probability and percentage of mobile water/oil in tight sandstone under certain conditions. The model have considered the key influencing factors, including pore size distribution, minerals, micro-wettability, roughness of pore wall, oil-water interface and environment conditions. Compared with common methods, we have introduced the intermingled fractal method and statistic theory to evaluate the probability of oil-water mobilization in tight sandstone, and ignored time consuming and less important point (like detailed oil/water distribution) in large scale. This can make our method to finish evaluate process quickly. The novel point of this research is that, in our method, there is no need to use pore extraction, meshing, iteration or waiting for iteration convergence, which will spend a lot of time and make the calculation complicated.

2. Methodology

2.1. General building process of 3D intermingled fractal model

To calculate the oil-water mobilization process in tight sandstone, we should rebuild the pore space first. Here we utilized an effective and efficient pore space representation and reconstitution method, called 3D-IFM method, which has been successfully presented in our previous works in detail (Li et al., 2017b, 2018a, 2019). In brief, there are three steps as follows:

The first is to represent micropores in tight sandstone. Tight sandstone possesses abundant micropores composed by interparticle, intragranular, clay, and dissolution pores, which greatly influence the multiphase flowing behavior. The original information of micropores in tight sandstone comes from scalable scanning electron microscopy (SEM) images. The scanning area can reach 400 μm × 400 μm with the highest resolution of 4 nm, indicating that the main pores in tight sandstone range from approximately 0.03 to 2 μm. After image segmentation, we can obtain the pore size distribution. Then, the IFU model is built. By adjusting the fractal parameters of sub-units, we can simulate the real porous media's pore size distribution in the IFU model. Finally, on the basis of the fractal parameters, we can build a 3D-IFU model for pore space in tight sandstone by using the basic iteration law, as shown in Fig. 1.

The second step it to represent minerals. Mineral components greatly influence the flowing behavior because of roughness and wettability. The original information of mineral distribution in tight sandstone comes from mineral(EDS/BES) images. The scanning area can also reach 400 μm × 400 μm with the highest resolution of 0.2 μm, which reaches the scale of mineral granules. From minneral images analysis results, we can easily recognize that the dominant minerals are quartz, calcite, illite, and chlorite. These four dominant minerals occupy 95% of the total minerals. Similarly, the IFU method is used to rebuild mineral distribution in space. The detailed processes can be found in our previous work.

The third step is to attach mineral information on pores by combing the 3D IFU model for micropores and minerals. As shown in Fig. 1, each pore wall will gain at least one mineral information by overlapping the pore distribution and mineral distribution. To simplify the calculation process, we suggest that one pore gains only one mineral characteristic. Within one pore, the mineral that possesses the greatest proportion on the wall is regarded as the mineral information for this pore. Finally, each pore gains mineral information. Finally, based on the fractal-based 3D space, we introduced the statistic theory to calculate the probability of oil-water mobilization.

2.2. Background theory of the oil-water mobilization calculation in intermingled fractal model

The 3D intermingled fractal model is a powerful tool to quickly evaluate the transport behavior in porous media. When this method is used in shale, the apparent permeability can be derived fast, which is helpful to analysis the influencing factors on non-Darcy effect in organic pores (Li et al., 2017b, 2018a). Similarly, when this method is used in tight sandstone, the relative permeability and related influences can be investigated in detail (Li et al., 2019).

The intermingled fractal units (IFU) and probabilistic capillary connectivity (PCC) algorithm are fundamental of multiphase mobilization calculation in intermingled fractal model. The IFU model is efficient to represent random pore distribution in porous media, mainly developed by Pia and Sanna (Pia, 2016; Pia and Sanna, 2014b; Pia et al., 2014, 2016). IFU model is intermingled by several sub-units with different fractal parameters. The sub-units are revised from the Sierpinski carpet. In the IFU model, one can simulate the real porous media's pore size distribution by adjusting the fractal parameters of sub-units. Once the model's pore size distribution matches the real porous media's distribution, the IFU model can be regarded as a representation of the real porous media. Thus, the complicated pore space in porous media can be simplified as the IFU model, which is contributed by the iteration of several fractal parameters. Detailed theories and explanations about IFU model can be found in Pia and Sanna (Pia, 2016; Pia and Sanna, 2014b; Pia et al., 2014, 2016); thus, we will not repeat them again here. Permeability is calculated from the revised capillary bundle method in Pia and Sanna's works. But we think that many parameters in Pia and Sanna's revised capillary bundle are not easy to be determined, like the tortuosity of tubes. And the capillary bundle ignores the mass transfer between pores, which is actually over simplified for the matrix. So we derived 3D structure, in which the revised Sierpinski carpet sub-units (2D) is replaced by the revised Menger sponge (3D). The 3D intermingled fractal model (3D-IFM) is more similar to real porous media compared with capillary bundle model, because 3D-IFM can avoid tortuosity estimation, which is hard to be determined objectively in capillary bundle model. Thus, the 3D-IFM can improve the accuracy and reduce uncertainty in calculation process. The new problem is, how to evaluate permeability for 3D-IFM. Marshall (1958) has mentioned a method based on pore connective calculation. The key to the PCC method is to represent permeability as a function of connecting probability. Cihan, Sukop, Tyner, Perfect, Huang (Cihan et al., 2009) has fully

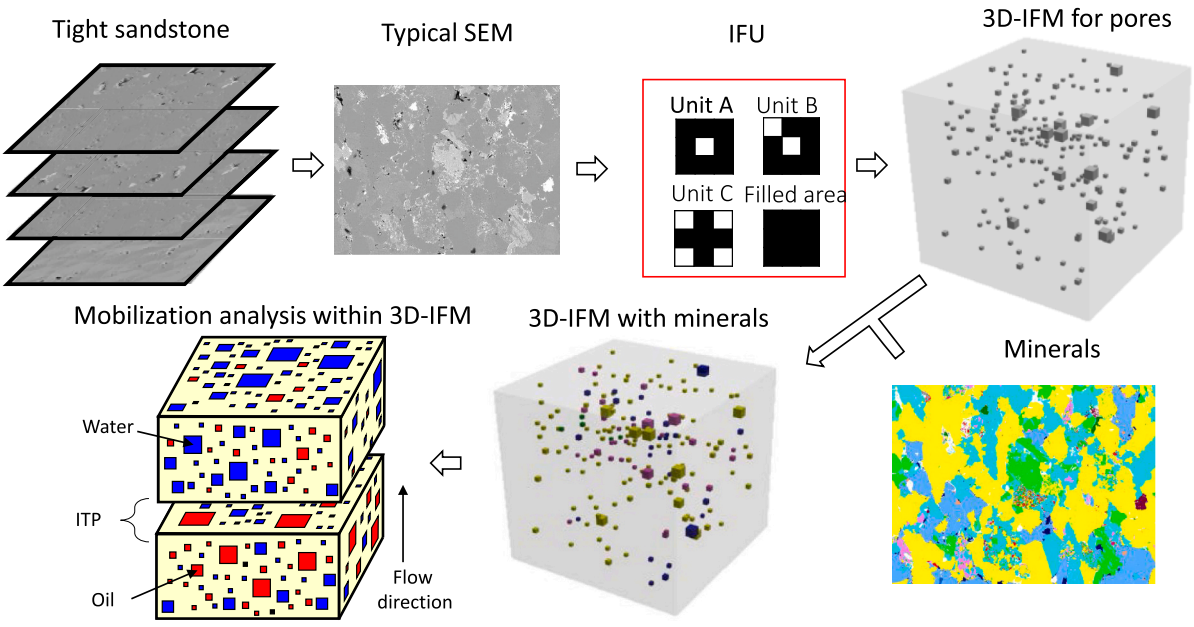

Fig. 1. General building process of 3D intermingled fractal model.

developed the method recently, but the scaling factor or fractal dimension of pore is a constant, which is not appropriate to the complex traverse scale and multi types of pores in unconventional matrix. The detailed process can be found in the mentioned works. So in 3D-IFM, we firstly combined PCC method with intermingled fractal structures, and given the method to calculate permeability and relative permeability (Li et al., 2018a, 2019). Here, we briefly repeat the basic laws of 3D-IFM, and additionally give the method to calculate the probability of oil-water mobilization.

Suggesting that the number of pores is sufficient; thus, any cross sections share the same fractal dimension and pore size distribution statistically. Fig. 2 shows a random horizontal cross section of porous media. The oil-water displacement direction is from bottom to top in this example. The cross section should be vertical to imbibition/displacement direction. For vertical cross sections, the method is the same. As illustrated in Fig. 2, the schematic has given six pores as an example. There are three kinds of pore diameters, from big one to small one as: λ_1, λ_2, λ_3. λ is the equivalent diameter. For λ_2 pores, there are three kinds: connecting pores with mineral 1 on pore wall, connecting pores with mineral 2 and dead ends. As illustrated, this example has two minerals on pore walls: mineral 1 and mineral 2. Each pore is simplified as one mineral on pore wall. For pores between different mineral grains, the dominant mineral is regarded as the mineral that controls the characteristic of pore wall.

There are two displacement methods, force displacement and imbibition. For force displacement, the matrix is filled with wetting phase first, and the non-wetting phase is driven in matrix to displace wetting phase. On the contrary, for imbibition process, the wetting phase will displace non-wetting phase spontaneously by capillary force. Take the force displacement for example. Suggesting that the pores in Fig. 2 gain water-wetting minerals on pore wall. The blue hatch means water (wetting phase) and red hatch means oil (non-wetting phase). The filled black block means dead ends, which will not participate in liquid transfer process. To finish the oil-water displacement process, two conditions should be fulfilled. The first is that, the pores in two sections should be connected to each other. The second is that, the oil-water interface have enough energy to travel across the pore neck. Based on probabilistic capillary connectivity theory (Marshall, 1958; Cihan et al., 2009), the connective probability for these pores can be classified as six parts: λ_1 pore on face A to λ_1 pore on face B, λ_1 pore on face A to λ_2 pore on face B, λ_1 pore on face A to λ_3 pore on face B, λ_2 pore on face A to λ_2 pore on face B, λ_2 pore on face A to λ_3 pore on face B, λ_3 pore on face A to λ_3 pore on face B. In summary, the probability can be expressed as:

$$P=\frac{\lambda_1^2}{A}\times\frac{\lambda_1^2}{A}+2\left(\frac{\lambda_1^2}{A}\times\frac{3\lambda_2^2}{A}\right)+2\left(\frac{\lambda_1^2}{A}\times\frac{\lambda_3^2}{A}\right)+\frac{3\lambda_2^2}{A}\times\frac{3\lambda_2^2}{A}+2\left(\frac{3\lambda_2^2}{A}\times\frac{\lambda_3^2}{A}\right)+\frac{\lambda_3^2}{A}\times\frac{\lambda_3^2}{A} \tag{1}$$

where A is the cross-sectional area of matrix. When it comes to multi-phase flow, things become complicated. The traverse probability from λ_1(face A) to λ_2(face B) and from λ_2(face A) to λ_1(face B) is different. Also, due to the wettability difference between mineral 1 and mineral 2, the λ_2(mineral 1) and λ_2(mineral 2) should be considered separately. So, the traverse probability P_2 is introduced to indicate the probability of meniscus travel over the pore neck, which is determined by the conflict between driving forces and resistance. $P_{2,i\to j}$ is the traverse probability from the λ_i level pore to the λ_j level pore. If driving forces can overcome the resistance, then $P_{2,i\to j}=1$, else $P_{2,i\to j}=0$. Based on the probabilistic capillary connectivity theory, in vertical force displacement process, P_2 can be expressed as (Li et al., 2019):

$$P_{2,i\to j}=\begin{cases}1 & \left(\Delta P-P_{c(i,j)}-\Delta D_{pf}\left[32\mu_{nw}L_p v\Big/\lambda_i^2+32\mu_w\left(L-L_p\right)v\Big/\lambda_j^2\right]-P_{initial}-P_G>0\right)\\ 0 & \left(\Delta P-P_{c(i,j)}-\Delta D_{pf}\left[32\mu_{nw}L_p v\Big/\lambda_i^2+32\mu_w\left(L-L_p\right)v\Big/\lambda_j^2\right]-P_{initial}-P_G<0\right)\end{cases} \tag{2}$$

Fig. 2. Pore connective calculation method considering minerals.

where ΔP is the driving force between inlet and outlet. ΔD_{pf} is the dimensionless roughness fraction on pore walls. The detailed explanations will be provided in the next section. μ_{nw} and μ_w refer to the viscosity of non-wetting and wetting phases, $P_{initial}$ is threshold pressure gradient, determined by Tian, Li, Ren, Josephine (Tian et al., 2018). P_G is gravity in vertical direction, commonly ignored in microscale for tight formation. $P_{c(i,j)}$ is capillary pressure, which can be expressed as

$$P_{c(i,j)} = \max\left[4\left(\tilde{C}_j\sigma_j\cos\theta_j\right)/\lambda_j, 4\left(\tilde{C}_i\sigma_i\cos\theta_i\right)/\lambda_i\right] \tag{3}$$

where $\tilde{C}$ is the curvature of a meniscus, σ is interfacial tension, θ is contact angle. Due to the difference between $P_{2,1\to2(m1)}$ and $P_{2,1\to2(m2)}$(m1 and m2 are mineral 1 and mineral 2 for short), an extended connecting probability calculation table is listed to separate three λ_2 into two λ_2 with mineral 1 and one λ_2 with mineral 2, shown in Table 1.

The general connecting and successful displacement probability P_{CSDP} is one of the fundamental parameter to calculate permeability and relative permeability. Based on the probabilistic capillary connectivity theory, the P_{CSDP} in Fig. 2(a) is:

$$P_{CSDP,1} = \left(\frac{\lambda_1^2}{A}\right)^2 \times P_{2,1(m1)\to1(m1)} \tag{4}$$

And in Fig. 2(b) and (c) can be expressed as:

$$P_{CSDP,2(m1)} = \frac{\lambda_1^2}{A}\frac{2\lambda_2^2}{A}P_{2,1(m1)\to2(m1)} + \frac{\lambda_1^2}{A}\frac{2\lambda_2^2}{A}P_{2,2(m1)\to1(m1)} + \frac{2\lambda_2^2}{A}\frac{2\lambda_2^2}{A}P_{2,2(m1)\to2(m1)} \tag{5}$$

And in Fig. 2(d)–(f) is:

$$P_{CSDP,2(m2)} = \frac{\lambda_1^2}{A}\frac{\lambda_2^2}{A}\left[P_{2,1(m1)\to2(m2)} + P_{2,2(m2)\to1(m1)}\right] + \frac{2\lambda_2^2}{A}\frac{\lambda_2^2}{A}\left[P_{2,2(m1)\to2(m2)} + P_{2,2(m2)\to2(m1)}\right]' + \left(\frac{\lambda_2^2}{A}\right)^2 P_{2,2(m2)\to2(m2)} \tag{6}$$

Similar expressions can be derived for λ_3 pores, it will not be expanded here. The detailed processes to calculate permeability based on P_{CSDP} can be found in Li, Lin, Ji, Jiang (Li et al., 2019). Here, as we focus on probability of oil-water mobilization. Based on probabilistic capillary connectivity theory, we introduced the P_{mob} to express the probability of oil-water mobilization, which is defined as: in displacement/imbibition process, the probability of pores filled in one phase being displaced successfully by another phase in a certain environment condition. P_{mob} is an efficient parameter to represent the multiphase mobilization behavior. Higher P_{mob} means that under the certain environment and pore structure condition, more pores will occur the multiphase displacement/imbibition process. P_{mob} is between 0 and 1. Similarly, $P_{mob,i}$ represents that for pores with the same iteration level i(equivalent diameter) but different minerals, the percentage of pores that will occur oil-water displacement/imbibition process. Based on the probabilistic capillary connectivity theory, the $P_{mob,1(m1)}$ (in Fig. 2(a)) can be expressed as:

$$P_{mob,1} = \frac{\lambda_1^2 \times P_{2,1(m1)\to1(m1)}}{\lambda_1^2} \tag{7}$$

Similarly, $P_{mob,2(m1)}$ (in Fig. 2(b)–(c)) can be expressed as:

$$P_{mob,2(m1)} = \frac{2\lambda_2^2 \times \left(P_{2,1(m1)\to2(m1)} + P_{2,2(m1)\to1(m1)} + 2P_{2,2(m1)\to2(m1)}\right)/4}{3\lambda_2^2} \tag{8}$$

And $P_{mob,2(m1)}$ (in Fig. 2(d)–(f)) can be expressed as:

$$P_{mob,2(m2)} = \frac{\lambda_2^2 \times \left(P_{2,1(m1)\to2(m2)} + P_{2,1(m2)\to2(m1)} + P_{2,2(m1)\to2(m2)} + P_{2,2(m2)\to2(m1)} + 2P_{2,2(m2)\to2(m2)}\right)/6}{3\lambda_2^2} \tag{9}$$

And $P_{mob,3(m2)}$ can also expressed based on the above theory and we ignored the illustrations in Fig. 2 and the related expressions.

Finally, the overall P_{mob} for the example in Fig. 2 can be expressed as:

$$P_{mob} = \frac{\lambda_1^2 P_{mob,1(m1)} + 3\left(\lambda_2^2 P_{mob,2(m1)} + P_{mob,2(m2)}\right) + \lambda_3^2 P_{mob,3(m2)}}{\lambda_1^2 + 3\lambda_2^2 + \lambda_3^2} \tag{10}$$

For a more general situation, in actual 3D-IFM, there are several kinds of pores with different wetting and roughness behaviors. So we have more general expressions for P_{CSDP}, permeability and relative permeability. Detailed expressions have shown in our previous works (Li et al., 2017b, 2018a, 2019). The following derivation briefly introduce the general equations of 3D-IFM presented in previous works, and then focus the way to express the probability of oil-water mobilization. First, the extended connecting probability calculation table can be listed as Table 1. The diameter column is rearranged in descending order ($\lambda_1 > \lambda_2 > \cdots > \lambda_n$). Within rows with the same diameter (like rows 1–4), the rows are rearranged in increasing order of capillary pressure. The

Table 1
Extended connecting probability calculation table.

Equivalent diameter	Mineral type	Number of pores	connected fraction	Capillary pressure
λ_1	Mineral 1	$N_{1(m1)}$	$P_{1,1(m1)}$	$P_{c,1(m1)}$
λ_1	Mineral 2	$N_{1(m2)}$	$P_{1,1(m2)}$	$P_{c,1(m2)}$
λ_1	Mineral 3	$N_{1(m3)}$	$P_{1,1(m3)}$	$P_{c,1(m3)}$
λ_1	Mineral 4	$N_{1(m4)}$	$P_{1,1(m4)}$	$P_{c,1(m4)}$
λ_2	Mineral 1	$N_{2(m1)}$	$P_{1,2(m1)}$	$P_{c,2(m1)}$
λ_2	Mineral 2	$N_{2(m2)}$	$P_{1,2(m2)}$	$P_{c,2(m2)}$
…	…	…	…	…
λ_n	Mineral 4	$N_{n(m4)}$	$P_{1,n(m4)}$	$P_{c,n(m4)}$

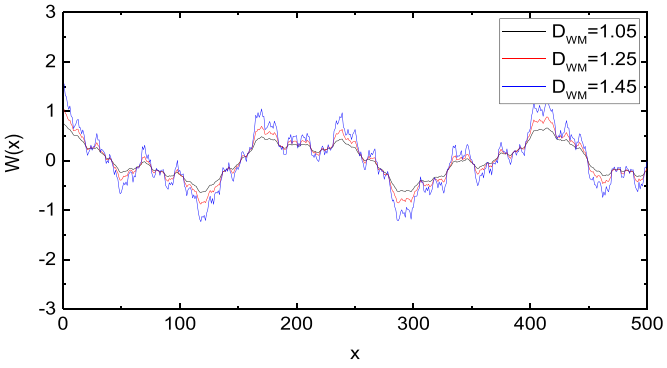

Fig. 3. The influence of D_{WM} on roughness.

reason of this arrangement is shown in (Li et al., 2018a, 2019). In Table 1, N_1 means the number of pores with diameter λ_1, $N_{1(m1)}$ means the number of pores with mineral 1 in λ_1 pores, so $N_1 = N_{1(m1)} + N_{1(m2)} + N_{1(m3)} + N_{1(m4)}$ in this example. $P_{1,1(m1)}$ means connected fraction, indicating the ratio of connecting pores to total pores (including dead ends) within iteration level 1 in mineral 1 pores. $\langle N_{1(m1)} P_{1,1(m1)} \rangle$ means the number of λ_1 pores with mineral 1 on pore walls. The angle brackets '< >' indicates nearest integer function, normally expressed as '[ ]'. But we replaced '[ ]' with '< >' to avoid ambiguous brackets in equations. So, considering the mineral and pore numbers, in more general 3D-IFM, the probability of oil-water mobilization for $\lambda_1$pores $P_{mob,1}$ can be expressed as:

$$P_{mob,1} = \frac{\sum_{i=1}^{4}\left\{\lambda_1^2\langle N_{1(mi)}P_{1,1(mi)}\rangle[1-S_{wres}(\alpha_{1(mi)},\theta_{1(mi)},1)]\sum_{j=1}^{i}\frac{P_{2,1(mj)\to 1(mi)}+P_{2,1(mi)\to 1(mj)}}{2i}\right\}}{\sum_{i=1}^{4}\lambda_1^2\langle N_{1(mi)}P_{1,1(mi)}\rangle} \tag{11}$$

where S_{wres} is the residual wetting phase percentage in cross section of pore. (Ma et al., 1996), Joekar-Niasar, Hassanizadeh (Joekar-Niasar and Hassanizadeh, 2012) have given the expressions as:

$$S_{wres} = \frac{\tan\alpha}{C_i^2}\left[\frac{\cos\theta_R}{\sin\alpha}\cos(\alpha+\theta_R) - \frac{\pi}{2}\left(1-\frac{\alpha+\theta_R}{90}\right)\right] \tag{12}$$

where α is the half angle of the corner in the cross section of pore, C_i is the shape factor for capillary at iteration level i, θ_R is the dynamic contact angle. The probability of oil-water mobilization for $\lambda_2$pores $P_{mob,2}$ can be expressed as:

$$P_{mob,2} = \frac{\sum_{i=1}^{4}\left\{\lambda_2^2\langle N_{2(mi)}P_{1,2(mi)}\rangle[1-S_{wres}(\alpha_{2(mi)},\theta_{2(mi)},2)]\frac{\sum_{j=1}^{4}\left(P_{2,2(mi)\to 1(mj)}+P_{2,1(mj)\to 1(mi)}\right)+\sum_{j=1}^{i}\left(P_{2,2(mi)\to 2(mj)}+P_{2,2(mj)\to 2(mi)}\right)}{2(4+i)}\right\}}{\sum_{i=1}^{4}\lambda_2^2\langle N_{2(mi)}P_{1,2(mi)}\rangle} \tag{13}$$

Similarly, the probability of oil-water mobilization for λ_n pores $P_{mob,n}$ can be expressed as:

$$P_{mob,n} = \frac{\sum_{i=1}^{4}\left\{\lambda_n^2\langle N_{n(mi)}P_{1,n(mi)}\rangle[1-S_{wres}(\alpha_{n(mi)},\theta_{n(mi)},n)]\frac{\sum_{k=1}^{n-1}\sum_{j=1}^{4}\left(P_{2,n(mi)\to k(mj)}+P_{2,k(mj)\to n(mi)}\right)+\sum_{j=1}^{i}\left(P_{2,2(mi)\to 2(mj)}+P_{2,2(mj)\to 2(mi)}\right)}{2[4\times(n-1)+i]}\right\}}{\sum_{i=1}^{4}\lambda_n^2\langle N_{n(mi)}P_{1,n(mi)}\rangle} \tag{14}$$

Noticed that in the extended connecting probability calculation table, the number of minerals is regarded as four. Actually, the number of minerals can be any integer, commonly larger than four. Suggesting that the number of minerals is *Num*, Eq. (13) can be rearranged as:

$$P_{mob,n} = \frac{\sum_{i=1}^{Num}\left\{\lambda_n^2\langle N_{n(mi)}P_{1,n(mi)}\rangle[1-S_{wres}(\alpha_{n(mi)},\theta_{n(mi)},n)]\frac{\sum_{k=1}^{n-1}\sum_{j=1}^{Num}\left(P_{2,n(mi)\to k(mj)}+P_{2,k(mj)\to n(mi)}\right)+\sum_{j=1}^{i}\left(P_{2,2(mi)\to 2(mj)}+P_{2,2(mj)\to 2(mi)}\right)}{2[Num\times(n-1)+i]}\right\}}{\sum_{i=1}^{Num}\lambda_n^2\langle N_{n(mi)}P_{1,n(mi)}\rangle} \tag{15}$$

Eqs.(11)–(15) represent the probability of oil-water mobilization in each iteration level. For overall probability in a 3D-IFM matrix, the P_{mob} can be expressed as:

$$P_{mob} = \frac{P_{mob,1}\sum_{i=1}^{Num}\lambda_1^2\langle N_{1(mi)}P_{1,1(mi)}\rangle + P_{mob,2}\sum_{i=1}^{Num}\lambda_2^2\langle N_{2(mi)}P_{1,2(mi)}\rangle + \ldots + P_{mob,n}\sum_{i=1}^{Num}\lambda_n^2\langle N_{n(mi)}P_{1,n(mi)}\rangle}{\sum_{j=1}^{n}\sum_{i=1}^{Num}\lambda_j^2\langle N_{j(mi)}P_{1,j(mi)}\rangle}$$

$$= \frac{\sum_{j=1}^{n}\left[P_{mob,j}\sum_{i=1}^{Num}\lambda_j^2\langle N_{j(mi)}P_{1,j(mi)}\rangle\right]}{\sum_{j=1}^{n}\sum_{i=1}^{Num}\lambda_j^2\langle N_{j(mi)}P_{1,j(mi)}\rangle} \quad (16)$$

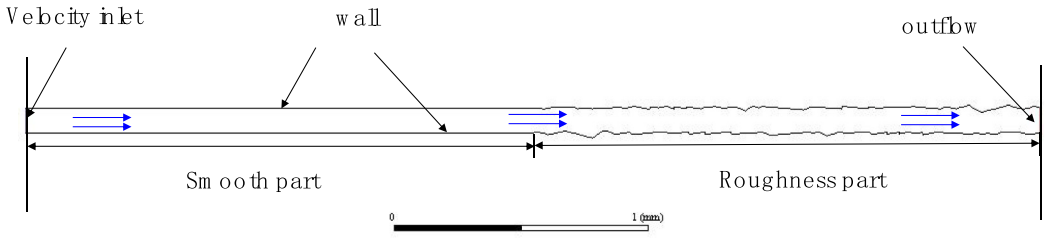

Fig. 4. The boundary conditions and meshing results.

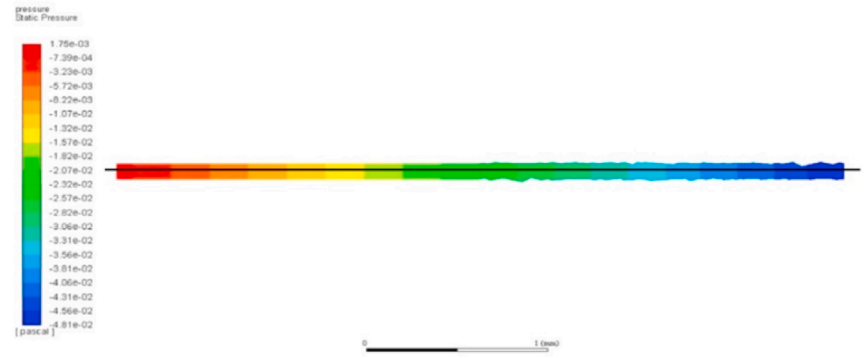

(a)

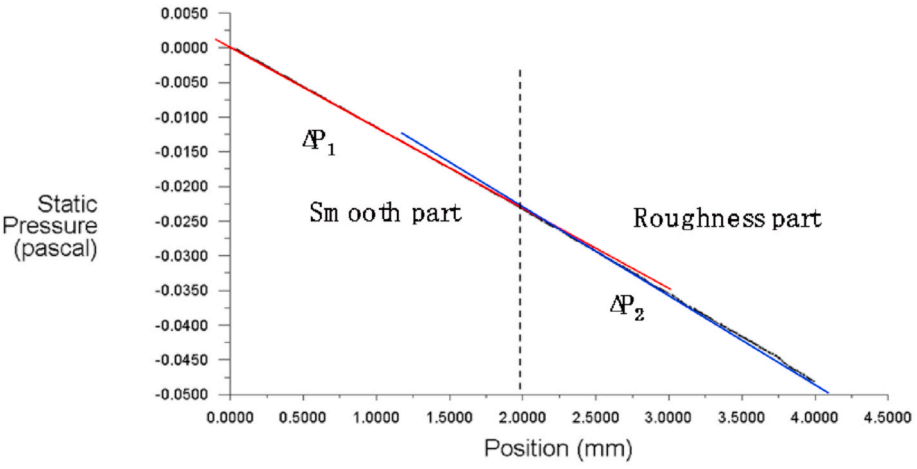

(b)

Fig. 5. The pressure distribution in roughness pore.

Table 2
Parameter combination table of dimensionless frictional pressure loss.

No.	D_{WM}	λ	ν	μ	$\triangle P$
1	1.25	0.1	0.001	1	1.07
2	… …	… …	… …	… …	… …
3	… …	… …	… …	… …	… …

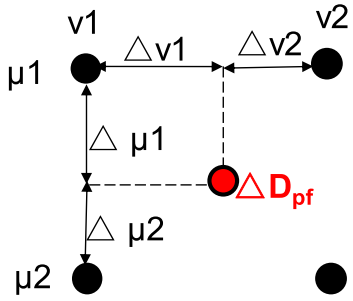

Fig. 6. The illustration of interpolation method.

2.3. Wettability on pore wall

Wetting characteristic on wall greatly influences the migration process. Most pores in tight sandstone range from 0.03 to 2 μm. Different minerals have diverse wetting properties. Tight sandstone consists of several mineral grains, such as quartz, albite, dolomite, orthoclase, and illite. During displacement, the wettability of these grains substantially influences the relative permeability and residual distribution. Each mineral features its own wettability property. Different contact angle features diverse capillary force; thus, contact angle influences the displacement behavior. Within pores in this scale, the capillary will greatly influence the multiphase migration, whether it is acting as a driving force (imbibition) or as a resistance (force displacement). The capillary item in Eq. (3) is mainly under the influence of the contact angle and pore diameter. In the 3D-IFM model, the contact angles of minerals are determined by a static contact angle test on two displacement phases. For example, in water–oil displacement, the contact angle of mineral is tested in a water–oil system.

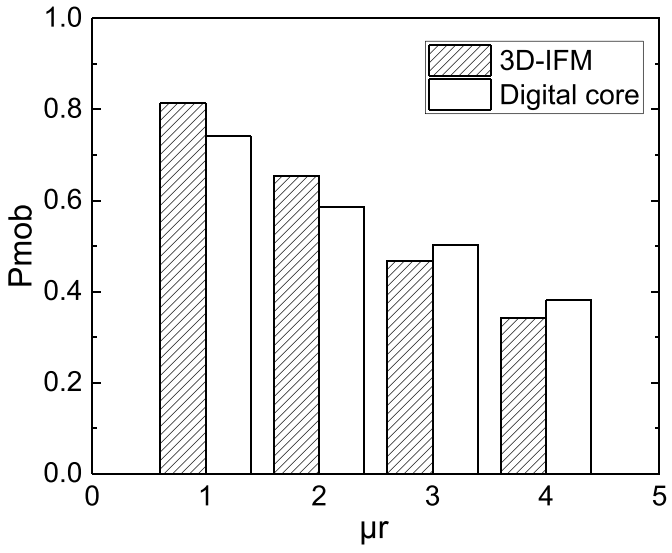

Fig. 7. The accuracy test for P_{mob} by comparing the 3D-IFM and digital core method.

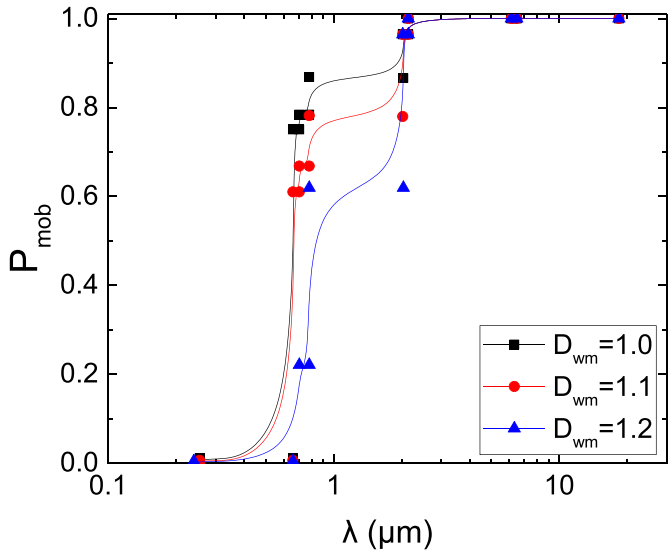

Fig. 8. The influence of roughness on probability of oil-water mobilization in different pore diameters.

2.4. Roughness and pressure loss on pore wall

Apart from wettability, roughness also influences the displacement process. During liquid flow in pores, roughness on the pore wall will change the streamline, thus increasing the flow resistance, decreasing the liquid energy, and finally influencing the displacement probability. In macro pores, the thickness of the rough layer is relatively small compared with the pore diameter. Thus, the influence of roughness on the pore wall can be ignored. By contrast, the rough layer in nanopores is not negligible. To calculate the influence of roughness on liquid, the key is to obtain the energy loss or pressure head loss on liquid. Generally, we use numerical method to calculate the pressure head loss.

The analytical expression of roughness and pressure loss is hard to get, so we use the numerical method. To achieve the steps above, we build a numerical model and recalculate the model by changing the influencing factors. We use the building process of one numerical model as an example. The first step is to generate the rough wall. Fractal dimension of roughnessD_{WM} influences the roughness, shown in Fig. 3. As D_{WM} increases from 1.05 to 1.45, the roughness increases greatly. The

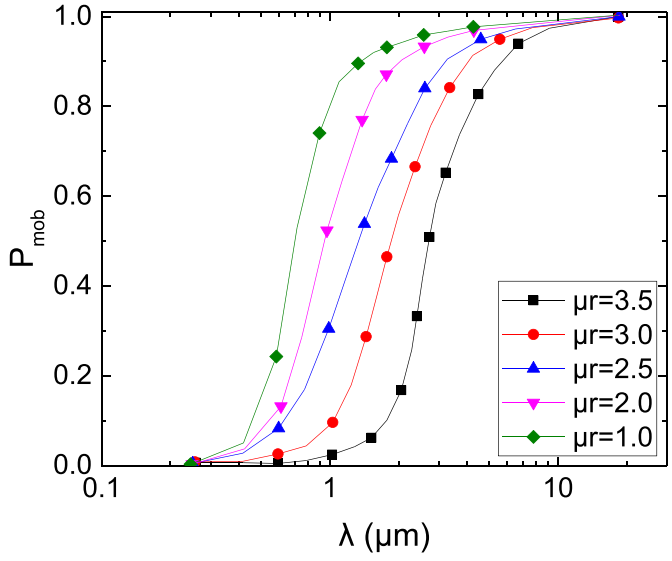

Fig. 9. The influence of viscosity on probability of oil-water mobilization in different pore diameters.

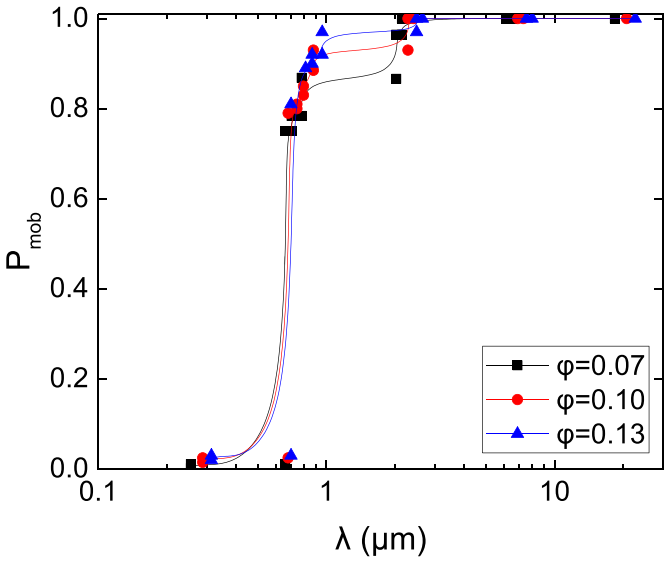

Fig. 10. The influence of porosity on probability of oil-water mobilization in different pore diameters.

D_{WM} can be determined from images in microscale. In numerical models, we can build the models with different D_{WM}.

The roughness of the pore wall can be represented by the Weierstrass–Mandelbrot function, which can be expressed as

$$W(x) = \sum_{k=1}^{\infty} \lambda^{(D_{WM}-2)k} \sin\left(\lambda^k x\right) \tag{17}$$

where $W(x)$ is the roughness function; λ is the periodic parameter, which is normally $\lambda > 1$. When λ is an integer, the roughness function $W(x)$ is a periodic function. The Weierstrass–Mandelbrot function also has a cosine expression (Majumdar and Tien, 1990; Maragos and Sun, 1996) as follows:

$$W(x) = \frac{\sum_{j=1}^{n} \sum_{k=1}^{\infty} \lambda^{(D_{WM,j}-2)k} \sin\left(\lambda_j{}^k x\right)}{\sum_{j=1}^{n} j} \tag{18}$$

The flow speed is relatively low in displacement. On the rough wall, the pressure loss is difficult to acquire analytically; thus, we use the numerical method. The steps are as follows:(1) A rough pore wall is generated by using the Weierstrass–Mandelbrot function; (2) A flow model is built by using the CFD method, (3) The boundary conditions are meshed and set, (4) Pressure loss on smooth and rough surfaces is calculated, follows by dimensionless pressure loss; (5) The influencing

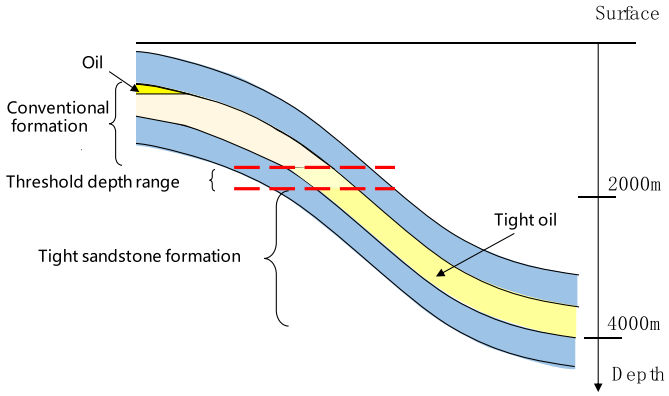

Fig. 11. The schematic of conventional formation and tight sandstone.

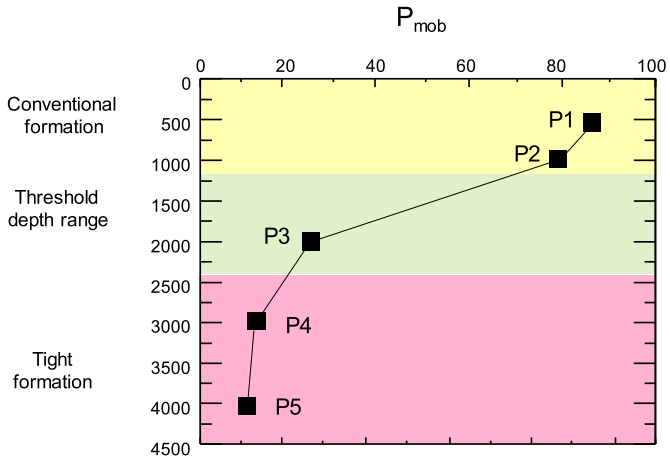

Fig. 12. The variation of P_{mob} with depth and related oil-water moveable range.

factors are changed and dimensionless pressure loss is recalculated by repeating steps (1) to (4); (6) A dimensionless pressure loss database is built, and pressure loss in real pores is calculated by linear interpolation.

On the basis of the generated rough wall, we build a numerical model. Fig. 4 shows the boundary conditions, which is meshed by using the tri + quad method. After initialization, the model can be calculated. Fig. 5 shows the pressure field and pressure drop. We can acquire the pressure loss within the pore. Clearly, the pressure loss in the rough part is heavier than in the smooth part. Dimensionless frictional pressure loss ΔD_{pf} can be calculated by the slope of the rough part divided by the slope of the smooth part.

$$\Delta D_{pf} = \frac{k_{f-rough}}{k_{f-smooth}} = \frac{\Delta P_{f-rough}/\Delta L_{rough}}{\Delta P_{f-smooth}/\Delta L_{smooth}} \tag{19}$$

From Fig. 5(b), we can calculate that ΔD_{pf} in this condition is 1.07. By changing the numerical model's roughness, pore diameter, velocity, and viscosity, we can obtain ΔD_{pf} within different parameter combinations, and build a parameter table, like Table 2.

In our 3D-IFM model, we use the multivariate interpolation method for random parameter combinations. For example, in two dimensional interpolation, if velocity between v_1 and v_2, viscosity between μ_1 and μ_2, at the same time, $\Delta D_{pf}(\mu_1, v_1)$, $\Delta D_{pf}(\mu_1, v_2)$, $\Delta D_{pf}(\mu_2, v_1)and\Delta D_{pf}(\mu_2, v_2)$ were derived by numerical simulation, then we can easily confirm unknown ΔP_{Df} by interpolation method. The illustration of interpolation method is shown in Fig. 6.

2.5. The accuracy of the oil-water mobilization probability

The multiphase displacement process in tight sandstone is complex, which is influenced by many factors, like the liquid behavior, mineral components, pore structure and connectivity. The intermingled fractal method is novel but efficient to estimate flowing behavior by combining the fractal theory and PCC method. In our previous works (Li et al., 2019), this method has a good application in the multiphase flow calculation process in tight sandstone.

We choose a small cube of sandstone (400 μm in edge length, with resolution 2μm/pixel) to test the accuracy of this method by comparing with the digital core method. In digital core method, the 3D cube is generated by MCMC method based on the 2D SEM images, and then calculating the stable state of displacement process. And finally, counting the number of pores with irreducible water to derive P_{mob}. Fig. 7 expresses the calculated P_{mob} for 3D-IFM and digital core method under different oil-water viscosity ratio, showing that the accuracy of P_{mob} by 3D-IFM is acceptable.

3. Influencing factors on micro-migration

In this section and the following sections, we used the previous built 3D-IFM for tight sandstone to investigate some important influencing factors in the multiphase displacement process.

3.1. Roughness on pore wall

Roughness is a special and important parameter for tight sandstone. We calculated the probability of oil-water mobilization P_{mob} under different pore diameter, and change the roughness of pores. The results are shown in Fig. 8. As pore diameter increases, P_{mob} gradually increases from 0.07 to 1. Between 0.3 and 2 μm, P_{mob} increases sharply, indicating that under the given condition, for pores larger than 2 μm, oil-water mobilization process will occur in a high probability. This range can be regarded as a threshold diameter, which is important for analyzing oil-water mobilization. For pores within the range 0.3–2 μm, as the fractal dimension of roughnessD_{WM} increases, the pore wall becomes rougher, the pressure loss on the wall increases, and P_{mob} decreases.

3.2. Fluid viscosity

Viscosity is another key influencing factor on the oil–water migration process. Fig. 9 shows the influence of viscosity on the probability of oil-water mobilization P_{mob}. We use the oil–water viscosity ratio to represent the influence of viscosity. Generally, P_{mob} is positive to pore size and negative to oil–water viscosity ratio. The boundary of the threshold diameter range is ambiguous. When the oil–water viscosity ratio is 1.0, the threshold diameter range is about 0.2–2 μm. When the oil–water viscosity ratio reaches 3.5, the threshold diameter range is about 2–6 μm. As the formation temperature increases, the oil–water viscosity ratio decreases, thereby causing the flow resistance to decrease. Under this circumstance, for some pores, especially within the range between 0.2 and 6 μm, the traverse probability increases, thereby causing P_{mob} to increase.

3.3. General porosity

Porosity is also an influencing factor on oil–water mobilization. To analysis the influence of porosity, we slightly expand and shrink all pores in general, and calculate the probability of oil-water mobilization in different pore diameters. From Fig. 10 we can conclude that under the given condition, the influence of porosity for different pores is slight in general. In larger pores, the influence is more obvious. Also, the threshold diameter for oil–water mobilization also exists. As the diameter increases from 0.6 to 1 μm under the given environment condition, the probability sharply increases from 0.3 to 1.0. This threshold diameter is an important parameter to analysis the oil–water mobilization process. If most pores in tight sandstone are smaller than the threshold diameter, the oil–water mobilization probability will be quite low, that is in this situation, wetting phase are ‘locked’ in matrix and barely displaced by non-wetting phase.

4. A Simple application: The probability of oil-water mobilization in tight sandstone formation

In normal sandstone, oil assembles at the top of the anticline, and water stays at the bottom because of gravity. In normal sandstone, most pores are large and the capillary resistance is much smaller than floatage. Thus, oil can overcome capillary force and other kinds of resistance and get assembled at the top of the anticline to form oil formation. As depth increases, the pores gradually becomes smaller, thereby increasing the capillary resistance. Once floatage cannot overcome resistance, oil–water will not form gravitational differentiation. This threshold depth is an important parameter for the tight oil formation development. The schematic of conventional formation and tight sandstone is shown in Fig. 11. On the basis of the 3D-IFM for tight sandstone, we calculated the overall probability of oil-water mobilization P_{mob} at different depths from 500 to 4000 m, considering the variation of formation pressure, temperature and pore space compression.

The results and related pore size distribution are shown in Fig. 12. Generally, at D = 500 m, within more than 90% pores, oil can displace water simply through buoyancy. As depth increases, P_{mob} decreases gradually. Under the given environment condition, P_{mob} decreases sharply at a depth ranging from 1000 to 2000 m, because within this rage, pores near peak range in pore size distribution change from buoyancy-movable into buoyancy-unmovable. Below 2000 m, the overall buoyancy displacement probability of oil-water mobilization is quite low. In most pores, oil cannot mobilize upwards and overcome resistance under the given environment condition. Thus, the depth range that causes P_{mob} to decrease sharply is called the up-lim of tight oil mobilization or the threshold depth range.

Threshold depth range is influenced by many parameters; in this paper, we mainly discuss the influence of geothermal gradient and pore pressure gradient. As geothermal gradient increases, the temperature difference increases as the depth increases. Fig. 13 illustrates that as the geothermal gradient increases from 2.0 to 3.0, P_{mob} generally increases from 10% to 50% at deep formation, and the range of the up-lim of tight sandstone is extended. Similarly, as the pressure gradient increases, P_{mob} gradually decreases, at the same time, the range of the up-lim slightly increase.

To be noticed, this application is just a very simple case about how the P_{mob} change with the depth. For highly heterogeneous reservoir, there may exist some ways to apply this technology, like: 1)we can focus on the layer we concern the most, and collect the samples, and then to change the liquid behavior parameters (like the viscosity of oil and water) or environment parameters (like temperature), to simulate how the oil-water mobilization probability will change when the liquid and environment parameter changes. 2) we can choose samples in adjacent (but different) production layers and use our method to build the models, and then compare the difference on mobilization probability difference between two layers (with different pore structure but the same temperature).

5. Conclusions

In this work, the 3D-IFM model for oil-water mobilization in tight sandstone is built. The model included the major influencing factors on oil-water mobilization, like mineral wettability, roughness, pore size distribution and environmental conditions. Based on this model, the probability of oil-water mobilization is derived based on pore connective calculation theory. Then, by calculating the mobilization probability under different depth, the influencing factors on up-lim of tight oil mobilization or the threshold depth range has been discussed. The findings show the following: First, 3D-IFM is useful and efficient for calculating oil-water mobilization in tight sandstone. Second, mineral wettability and roughness, pore size distribution, and environmental conditions are the main influencing factors for multiphase migration. A threshold diameter for oil–water mobilization exists. Finally, with the increase in depth, the probability of oil-water mobilization decreases. A sharp decrease in probability also exists, called the up-lim of tight oil mobilization or the threshold depth range of tight oil formation. With the increase in geothermal gradient or decrease information pressure gradient, the up-lim range of tight oil formation decreases.

Credit author statement

Caoxiong Li, wrote the manuscript, Mian Lin and Chenggang Xian, designed the manuscript, Jing Liu, Lili Ji and Wenbin Jiang, were helpful for the resources and the calculation of this manuscript.

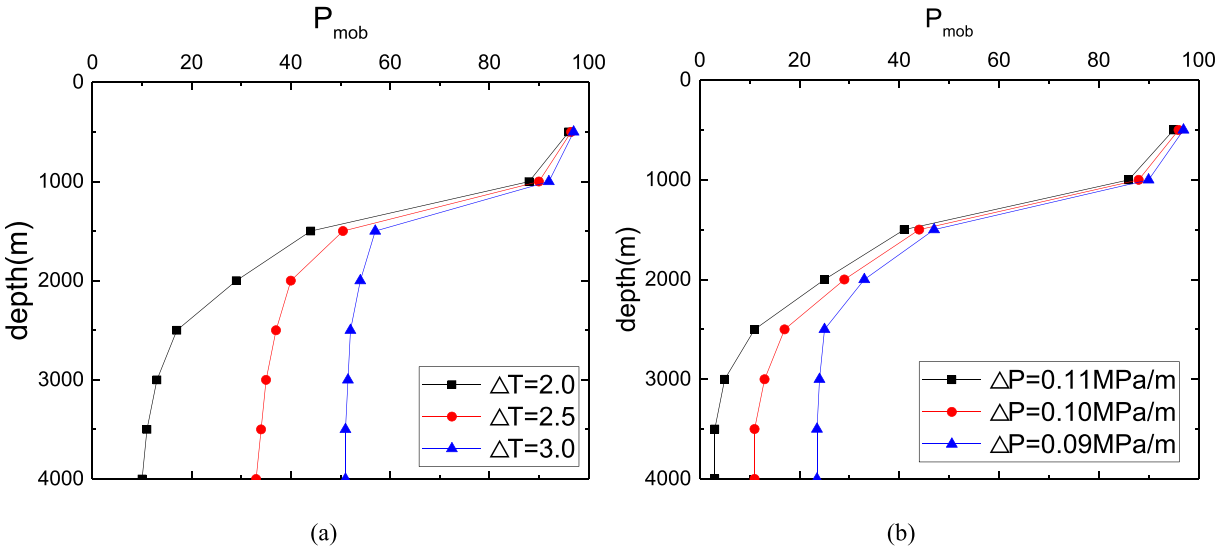

Fig. 13. The influence of temperature and pore pressure on P_{mob} in different depth.

Declaration of competing interest

The authors declare that they have no competing financial interests.

Acknowledgements

This work is supported by the Science Foundation of China University of Petroleum, Beijing (No. 2462020XKBH004), National Natural Science Foundation of China (Grant No. 41690132), the Strategic Priority Research Program of the Chinese Academy of Sciences (Grant No. XDA14010101) and the Major National Science and Technology Special Program of China (Grant No. 2017ZX05037-001).

Appendix A. Supplementary data

Supplementary data to this article can be found online at https://doi.org/10.1016/j.petrol.2020.107661.

References

Balankin, A.S., Elizarraraz, B.E., 2012a. Hydrodynamics of fractal continuum flow. Phys. Rev. 85 (2), 025302.
Balankin, A.S., Elizarraraz, B.E., 2012b. Map of fluid flow in fractal porous medium into fractal continuum flow. Phys. Rev. 85 (5), 056314.
Blunt, M.J., 1997. Effects of heterogeneity and wetting on relative permeability using pore level modeling, 0 SPE J. 2 (1), 70–87.
Bryant, S., Cade, C., 1992. Permeability Prediction from Geological Models. ECMOR III-3rd European Conference on the Mathematics of Oil Recovery.
Cai, J., Li, C., Song, K., Zou, S., Yang, Z., Shen, Y., et al., 2020. The influence of salinity and mineral components on spontaneous imbibition in tight sandstone. Fuel 269, 117087. https://www.sciencedirect.com/science/article/pii/S001623612030082X.
Cihan, A., Sukop, M.C., Tyner, J.S., Perfect, E., Huang, H., 2009. Analytical predictions and lattice Boltzmann simulations of intrinsic permeability for mass fractal porous media. Vadose Zone J. 8 (1), 187.
Erzan, A., Güngör, N., 1995. Fractal geometry and size distribution of clay particles. J. Colloid Interface Sci. 176 (2), 301–307.
Ghanbarian, B., Torres-Verdín, C., Skaggs, T.H., 2016. Quantifying tight-gas sandstone permeability via critical path analysis. Adv. Water Resour. 92, 316–322.
Joekar-Niasar, V., Hassanizadeh, S.M., 2012. Analysis of fundamentals of two-phase flow in porous media using dynamic pore-network models: a review. Crit. Rev. Environ. Sci. Technol. 42 (18), 1895–1976.
Katz, A., Thompson, A., 1985. Fractal sandstone pores: implications for conductivity and pore formation. Phys. Rev. Lett. 54 (12), 1325.
Krakowska, P., 2019. Detailed parametrization of the pore space in tight clastic rocks from Poland based on laboratory measurement results. Acta Geophysica 67 (6), 1765–1776.
Krakowska, P., Madejski, P., Jarzyna, J., 2014. Permeability estimation using CFD modeling in tight Carboniferous sandstone. 76th EAGE Conference and Exhibition, 2014.
Lai, J., Wang, G., 2015. Fractal analysis of tight gas sandstones using high-pressure mercury intrusion techniques. J. Nat. Gas Sci. Eng. 24, 185–196.
Li, C., Lin, M., Ji, L., Jiang, W., Cao, G., 2018a. Rapid evaluation of the permeability of organic-rich shale using the 3D intermingled-fractal model. SPE J. 23 (6), 2175–2187.
Li, P., Zheng, M., Bi, H., Wu, S., Wang, X., 2017a. Pore throat structure and fractal characteristics of tight oil sandstone: a case study in the Ordos Basin, China. J. Petrol. Sci. Eng. 149, 665–674.
Li, C., Lin, M., Ji, L., Jiang, W., Cao, G., 2017b. Investigation of intermingled fractal model for organic-rich shale. Energy & Fuels 31 (9), 8896–8909.
Li, Y., Li, H., Cai, J., Ma, Q., Zhang, J., 2018b. The dynamic effect in capillary pressure during the displacement process in ultra-low permeability sandstone reservoirs. Capillarity 1 (2), 11–18.
Li, C., Lin, M., Ji, L., Jiang, W., 2019. Multiphase flow in tight sandstone: an improved application for 3D intermingled fractal model. J. Petrol. Sci. Eng. 177, 403–414.
Liu, X., Kang, Y., Luo, P., You, L., Tang, Y., Kong, L., 2015. Wettability modification by fluoride and its application in aqueous phase trapping damage removal in tight sandstone reservoirs. J. Petrol. Sci. Eng. 133, 201–207.
Lu, T., Li, Z., Lai, F., Meng, Y., Ma, W., 2018. The effect of flow resistance on water saturation profifile for transient two-phase flow in fractal porous media. Advances in Geo-Energy Research 2 (1), 63–71.
Ma, S., Mason, G., Morrow, N.R., 1996. Effect of contact angle on drainage and imbibition in regular polygonal tubes. Colloid. Surface. Physicochem. Eng. Aspect. 117 (3), 273–291.
Majumdar, A., Tien, C., 1990. Fractal characterization and simulation of rough surfaces. Wear 136 (2), 313–327.
Mani, V., Mohanty, K., 1998. Pore-level network modeling of three-phase capillary pressure and relative permeability curves, 0 SPE J. 3 (3), 238–248.
Maragos, P., Sun, F.-K., 1996. Measuring the fractal dimension of signals: morphological covers and iterative optimization. SPIE MILESTONE SERIES MS 127, 506–519.
Marshall, T.J., 1958. A Relation between permeability and size distribution of pores. J. Soil Sci. 9 (1), 1–8.
Masters, J.A., 1979. Deep basin gas trap, western Canada. AAPG Bull. 63 (2), 152–181.
Meng, Qingbang, Cai, Zhongxian, Cai, Jianchao, et al., 2019. Oil recovery by spontaneous imbibition from partially water-covered matrix blocks with different boundary conditions. J. Petrol. Sci. Eng. 172, 454–464.
Pia, G., 2016. Fluid flow in complex porous media: experimental data and IFU model predictions for water vapour permeability. J. Nat. Gas Sci. Eng. 35, 283–290.
Pia, G., Sanna, U., 2014a. An intermingled fractal units model and method to predict permeability in porous rock. Int. J. Eng. Sci. 75, 31–39.
Pia, G., Sanna, U., 2014b. An intermingled fractal units model to evaluate pore size distribution influence on thermal conductivity values in porous materials. Appl. Therm. Eng. 65 (1–2), 330–336.
Pia, G., Sassoni, E., Franzoni, E., Sanna, U., 2014. Predicting capillary absorption of porous stones by a procedure based on anintermingled fractal units model. Int. J. Eng. Sci. 82, 196–204.
Pia, G., Siligardi, C., Casnedi, L., Sanna, U., 2016. Pore size distribution and porosity influence on Sorptivity of ceramic tiles: from experimental data to fractal modelling. Ceram. Int. 42 (8), 9583–9590.
Shao, X., Pang, X., Jiang, F., Li, L., Huyan, Y., Zheng, D., 2017a. Reservoir characterization of tight sandstones using nuclear magnetic resonance and incremental pressure mercury injection experiments: implication for tight sand gas reservoir quality. Energy & Fuels 31 (10), 10420–10431.
Shao, X., Pang, X., Li, H., Zhang, X., 2017b. Fractal analysis of pore network in tight gas sandstones using NMR method: a case study from the Ordos basin, China. Energy & Fuels 31 (10), 10358–10368.
Sheng, Guanglong, Su, Yuliang, Wang, Wendong, 2019. A new fractal approach for describing induced-fracture porosity/permeability/compressibility in stimulated unconventional reservoirs. J. Petrol. Sci. Eng. 179, 855–866.

Spencer, C.W., 1989. Review of characteristics of low-permeability gas reservoirs in western United States. AAPG Bull. 73 (5), 613–629.
Tang, X., Jiang, Z., Jiang, S., Li, Z., 2016. Heterogeneous nanoporosity of the Silurian Longmaxi Formation shale gas reservoir in the Sichuan Basin using the QEMSCAN, FIB-SEM, and nano-CT methods. Mar. Petrol. Geol. 78, 99–109.
Tian, W., Li, A., Ren, X., Josephine, Y., 2018. The threshold pressure gradient effect in the tight sandstone gas reservoirs with high water saturation. Fuel 226, 221–229.
Wang, X., Sheng, J.J., 2018. Pore network modeling of the Non-Darcy flows in shale and tight formations. J. Petrol. Sci. Eng. 163, 511–518.
Wang, X., Yin, H., Zhao, X., Li, B., Yang, Y., 2019. Microscopic remaining oil distribution and quantitative analysis of polymer flooding based on CT scanning. Advances in Geo-Energy Research 3 (4), 448–456.
Xiao, D., Jiang, S., Thul, D., Lu, S., Zhang, L., Li, B., 2018. Impacts of clay on pore structure, storage and percolation of tight sandstones from the Songliao Basin, China: implications for genetic classification of tight sandstone reservoirs. Fuel 211, 390–404.
Yan, W., Sun, J., Golsanami, N., Li, M., Cui, L., Dong, H., et al., 2019. Evaluation of wettabilities and pores in tight oil reservoirs by a new experimental design. Fuel 252, 272–280.
Yong, H., Xizhe, L., Yujin, W., Jiangliang, L., Huayin, Z., Zhang, Y., et al., 2013. Physical simulation on gas percolation in tight sandstones. Petrol. Explor. Dev. 40 (5), 621–626.
Zhang, Z., Weller, A., 2014. Fractal dimension of pore-space geometry of an Eocene sandstone formation. Geophysics 79 (6), D377–D387.
Zhang, Y., Chen, M., Jin, Y., Lu, Y., Liang, C., Li, W., et al., 2016. Experimental study and artificial neural network simulation of the wettability of tight gas sandstone formation. J. Nat. Gas Sci. Eng. 34, 387–400.
Zhang, L., Lu, S., Xiao, D., Li, B., 2017. Pore structure characteristics of tight sandstones in the northern Songliao Basin, China. Mar. Petrol. Geol. 88, 170–180.
Zhang, Yongchao, Zeng, Jianhui, Cai, Jianchao, et al., 2019. Mathematical model for determining oil migration characteristics in low-permeability porous media based on fractal theory. Transport Porous Media 129 (3), 633–652.
Zhao, H., Ning, Z., Wang, Q., Zhang, R., Zhao, T., Niu, T., et al., 2015. Petrophysical characterization of tight oil reservoirs using pressure-controlled porosimetry combined with rate-controlled porosimetry. Fuel 154, 233–242.
Zhou, L., Kang, Z., 2016. Fractal characterization of pores in shales using nmr: a case study from the lower cambrian niutitang formation in the middle yangtze platform, southwest China. J. Nat. Gas Sci. Eng. 35, 860–872.